Enhanced mercury reduction in the South Atlantic Ocean during carbon remineralization

Igor Živković [a,*], Matthew P. Humphreys [b], Eric P. Achterberg [c], Cynthia Dumousseaud [d], E. Malcolm S. Woodward [e], Natalia Bojanić [f], Mladen Šolić [g], Arne Bratkič [h], Jože Kotnik [a,i], Mitja Vahčič [j], Kristina Obu Vazner [i,k], Ermira Begu [a], Vesna Fajon [a,i], Yaroslav Shlyapnikov [a,i], Milena Horvat [a,i]

[a] Department of Environmental Sciences, Jožef Stefan Institute, Jamova cesta 39, 1000 Ljubljana, Slovenia
[b] NIOZ Royal Netherlands Institute for Sea Research, Department of Ocean Systems (OCS), P.O. Box 59, 1790 AB Den Burg, Texel, the Netherlands
[c] GEOMAR Helmholtz Centre for Ocean Research Kiel, Wischhofstraße 1–3, 24148 Kiel, Germany
[d] Ocean and Earth Science, National Oceanography Centre Southampton, University of Southampton Waterfront Campus, European Way, Southampton SO14 3ZH, United Kingdom
[e] Plymouth Marine Laboratory, Prospect Place, Plymouth PL1 3DH, United Kingdom
[f] Laboratory of Plankton and Shellfish Toxicity, Institute of Oceanography and Fisheries, Šetalište I. Meštrovića 63, 21000 Split, Croatia
[g] Laboratory of Marine Microbiology, Institute of Oceanography and Fisheries, Šetalište I. Meštrovića 63, 21000 Split, Croatia
[h] Chemistry Department, Vrije Universiteit Brussel, Pleinlaan 2, 1050 Elsene, Belgium
[i] Jožef Stefan International Postgraduate School, Jamova cesta 39, 1000 Ljubljana, Slovenia
[j] Joint Research Centre, European Commission, Retieseweg 111, 2440 Geel, Belgium
[k] Ecological Engineering Institute, Ljubljanska ulica 9, 2000 Maribor, Slovenia

ARTICLE INFO

ABSTRACT

Mercury (Hg) in seawater is subject to interconversions via (photo)chemical and (micro)biological processes that determine the extent of dissolved gaseous mercury (DGM) (re)emission and the production of mono-methylmercury. We investigated Hg speciation in the South Atlantic Ocean on a GEOTRACES cruise along a 40°S section between December 2011 and January 2012 (354 samples collected at 24 stations from surface to 5250 m maximum depth). Using statistical analysis, concentrations of methylated mercury (MeHg, geometric mean 35.4 fmol L^{-1}) were related to seawater temperature, salinity, and fluorescence. DGM concentrations (geometric mean 0.17 pmol L^{-1}) were related to water column depth, concentrations of macronutrients and dissolved inorganic carbon (DIC). The first-ever observed linear correlation between DGM and DIC obtained from high-resolution data indicates possible DGM production by organic matter remineralization via biological or dark abiotic reactions. DGM concentrations projected from literature DIC data using the newly discovered DGM–DIC relationship agreed with published DGM observations.

1. Introduction

Mercury (Hg) is a toxic global contaminant, with enhanced surface ocean concentrations due to elevated anthropogenic Hg emissions and subsequent deposition in the oceans (Mason et al., 1994). Two main groups of reactions affecting Hg speciation in the marine environment are redox and methylation/demethylation reactions. The reduction of oxidized Hg species in the surface ocean can result in (re)emission to the atmosphere (Costa and Liss, 1999; Gårdfeldt et al., 2003; Mason et al., 1994), while methylation produces monomethylmercury and dimethylmercury (DMeHg) (Compeau and Bartha, 1987; Matsuyama et al., 2021).

The production of dissolved gaseous mercury (DGM; mostly composed of dissolved elemental Hg – dHg^0) in surface waters is mostly due to photochemical Hg^{II} reduction (Monperrus et al., 2007). Sea surface temperature has been used as a seasonal proxy for dHg^0 production in near-surface waters (Chen et al., 2020). DGM production has also been related to photodegradation of methylated mercury (MeHg) (M.-K. Kim et al., 2016), bacterial Hg reduction under dark conditions (Fantozzi et al., 2009; Joshi et al., 2021), phytoplankton photosynthetic

---

* Corresponding author.
  E-mail address: igor.zivkovic@ijs.si (I. Živković).

activity (Poulain et al., 2004), and degradation of labile terrestrial organic matter (Oh et al., 2011; Schartup et al., 2015).

Photochemical reduction occurs through the homolysis of Hg complexes with dissolved organic matter (DOM) or through secondary reactions with reactive reductants via highly reactive radical intermediates (Zheng and Hintelmann, 2010). Phototrophs might be involved in Hg^{II} reduction via their photosynthetic machinery or through the release of photoreactive compounds (Grégoire and Poulain, 2014). Phototrophs can also use Hg^{II} as an electron sink to maintain redox homeostasis (Grégoire and Poulain, 2016). Turnover of labile terrestrial organic matter can reduce the stability of Hg bound to DOM, which enhances Hg^{II} reduction rates (Schartup et al., 2015). Hg^{II} in the dark ocean can be reduced by reactive oxygen species (produced by marine heterotrophs) or by Mn^{III} in seawater (Lamborg et al., 2021). In anoxic (micro)environments, Hg^{II} can be effectively reduced in the presence of small amounts of humic acid (Gu et al., 2011) by electron transfer from the reduced quinone moieties (semiquinone or hydroquinone) (Zheng et al., 2012; Zheng and Hintelmann, 2010).

Hg methylation in the upper ocean has been linked to organic carbon remineralization and heterotrophic microbial activity (Cossa et al., 2009, 2011; Heimbürger et al., 2010; Sunderland et al., 2009). Carbon remineralization rates are enhanced during sinking of fresh material from decaying picocyanobacterial bloom (Bach et al., 2019). Organic particles formed at the surface serve as a sink for Hg that is not (re) emitted to the atmosphere (Cossa et al., 2009; Strode et al., 2010). At depth, Hg is released during remineralization. The participation of Hg in the biological pump has been used to predict the vertical distribution of anthropogenic Hg in the ocean (Strode et al., 2010). However, the effects of organic matter remineralization on the reduction of inorganic Hg^{II} and DGM production are not well documented.

Atmospheric carbon dioxide (CO_2) and Hg are taken up by the oceans. Absorbed CO_2 is incorporated into dissolved organic matter (DOM) and particulate organic matter (POM), with transfer to depth and subsequent remineralization providing dissolved inorganic carbon (DIC) to the deep ocean, and also transferred to the deep sea by the solubility pump (Hansell and Carlson, 2015). As part of the biological carbon pump, DIC and inorganic nutrients are converted into organic matter in the upper ocean, which is exported to the deeper ocean via sinking particles and physical mixing processes (Giering and Humphreys, 2017). The organic matter is gradually remineralized, returning DIC and the accompanying nutrients to solution, and increasing their concentrations in the deeper ocean (Hansell and Carlson, 2015). Remineralization consumes oxygen and decreases the pH of seawater. The consumed amount of oxygen is proportional to the amount of nutrients and DIC released and represents a fundamental metric of the biological pump (Lea, 2014).

Microbial and abiotic reactions that cause the production and the removal of DOM are mutually interconnected. Heterotrophic production and the microbial loop are mainly driven by labile DOM. Labile DOM can be produced by photoautotrophs and by photochemical oxidation of upwelling refractory organic matter (which also produces DIC). Ultraviolet light can transform DOM to biologically available compounds, thus facilitating the uptake and remineralization of DOM by heterotrophic bacteria (Hansell and Carlson, 2015). Grazing, cell lysis, and cellular physiological processes can also release additional labile DOM. The microbial loop consumes labile DOM and converts it into DIC and inorganic nutrients (Hansell and Carlson, 2015). Different biotic and abiotic controls on heterotrophic bacteria affect their roles in nutrient cycling and in the transformation of organic matter. Sorption of DOM onto sinking particles is another abiotic removal mechanism. Physical disaggregation of these sinking particles release DOM into deep waters where it can be enzymatically degraded (Hansell and Carlson, 2015).

On the other hand, deposited Hg (mostly as Hg^{II}) can be photoreduced in the surface ocean and re-emitted to the atmosphere, incorporated within the biological pump, or complexed with sinking organic matter and possibly reduced to dHg^0 during organic matter remineralization at depth. In addition to these processes, mixing of oceanic water masses carrying different levels of Hg can cause changes in ambient Hg concentrations at depth (Sunderland and Mason, 2007); the same can be observed for DIC concentrations (Humphreys et al., 2016c).

The main objective of this study was to examine DGM formation in the South Atlantic Ocean along 40°S. The main questions were (i) whether environmental variables can be used as a proxy for DGM concentration, (ii) what possible mechanisms are involved in DGM formation, and (iii) whether these proxies can estimate DGM concentrations in different ocean regions. Using multivariate statistical analysis (principal component analysis), we determined which variables were correlated with different Hg fractions. These variables were related to known processes to explain Hg transformations, specifically Hg reduction in seawater. To test whether Hg reduction might be associated with mineralization of organic matter, we used high-resolution DIC data instead of more commonly used dissolved organic carbon/matter (DOC/DOM) data. Finally, we assessed the use of macronutrient data as a proxy for DGM concentrations in the deep sea.

2. Materials and methods

2.1. Study area, analytical methods, and data availability

This research is focused on a zonal South Atlantic cruise transect along 40°S, between Cape Town, South Africa and Montevideo, Uruguay (Fig. S1; Supplementary data) and carried out during December 2011 and January 2012 as part of the UK GEOTRACES program. The details on determination of Hg speciation, macronutrients and other environmental variables have been published by Bratkič et al. (2016) (the overview of section plots are presented in Fig. S2 for Hg species and Fig. S3 for macronutrients and temperature). DIC and total alkalinity (TA) have been reported by Humphreys et al. (2016a). Datasets for Hg (Bratkič and Vahčič, 2015) and DIC (Humphreys et al., 2016b) used in this work are publicly available online at https://doi.org/10/629 and https://doi.org/10/bjgs, respectively.

In brief, concentrations of total mercury (THg) in water were determined by cold vapor atomic fluorescence spectrometry (CVAFS) after BrCl digestion, UV irradiation and reduction with SnCl$_2$. DGM was determined by CVAFS after purging, collection on a gold trap with subsequent desorption. MeHg (sum of monomethylmercury and dimethylmercury) was determined by CVAFS after distillation, aqueous phase ethylation, collection on Tenax traps, desorption and subsequent pyrolysis (Bratkič et al., 2016). DIC was extracted from samples as CO_2 by the addition of phosphoric acid and determined following transfer using nitrogen gas of the evolved CO_2 to a coulometer. TA was determined by potentiometric titration with hydrochloric acid and calculated from the titration data using a modified Gran plot approach (Humphreys, 2015; Humphreys et al., 2016a).

DGM concentrations used for the comparison are from H. Kim et al. (2016), Kotnik et al. (2007), and two oceanographic campaigns in the Mediterranean Sea (unpublished data from Med-Oceanor 2015 and 2017). DGM in these samples was determined using the method described above.

2.2. Assessment of biological (remineralization) contribution to DIC

In this paper, the relationship between organic matter remineralization and DGM concentrations was estimated using DIC as a proxy. Quantification of the biological (remineralization) contribution to DIC requires correction for the preformed DIC (DIC$_{preformed}$; DIC present during the last contact with the atmosphere) (Sabine and Tanhua, 2010). Biologically mediated changes in DIC (DIC$_{bio}$) are due to dissolution of biogenic carbonates and remineralization of organic matter at depth (Körtzinger et al., 2003). Therefore, DIC$_{bio}$ is the difference between DIC and DIC$_{preformed}$, and can be estimated as: DIC$_{bio}$ = 0.798 × AOU + 0.5

$\times$ (TA $-$ TA^0), where AOU is apparent oxygen utilization, TA is measured total alkalinity and TA^0 is preformed total alkalinity. AOU was calculated from dissolved oxygen concentrations and oxygen solubility (Garcia and Gordon, 1992), while TA^0 was estimated from salinity and potential temperature (Körtzinger et al., 2003).

Preformed DGM was estimated using the temperature-dependent Henry's law (Andersson et al., 2008) for Hg^0 and assuming the atmospheric DMeHg concentration to be zero. To calculate preformed DGM in surface waters, we used current values for total gaseous Hg in the South Atlantic air (6.53 pmol m^{-3}) (Slemr et al., 2003). For deep waters, we assumed that the atmospheric Hg^0 concentrations at the time when these water masses were in the last contact with the atmosphere were four-fold lower than present-day values. This factor (four-fold) is an estimation calculated as a geometric mean of the enrichment factors for present-day-to-preindustrial and present-day-to-natural atmospheric mercury budgets (Amos et al., 2013). In our analysis, DGM was not corrected for its preformed values due to several issues. First, estimated preformed DGM in the South Atlantic was always low and constant (geometric mean 0.02 pmol L^{-1}). Next, to compare calculated DGM values with measured DGM values, we would require calculation of preformed DGM for various water masses across the globe. This would require information of when and where was a specific water mass last time in the contact with the atmosphere and what were the corresponding water temperature and atmospheric Hg^0 concentration. Due to impracticality/infeasibility of the determination of generally low values of preformed DGM, we decided not to correct DGM for its preformed values.

2.3. Statistical analysis

The normality of original and log-transformed data was tested using the Shapiro–Wilk test. As a normal distribution was not found in either case ($p < 0.05$), non-parametric statistical tests were used throughout the paper. Spearman's rank correlation coefficient (ρ) was used to assess relationships between DGM (MeHg) and environmental variables. Outliers in the dataset were removed using the Dixon test.

Principal Component Analysis (PCA) was performed to summarize the main patterns of variation between three Hg species (DGM, THg and MeHg) as active variables, and environmental variables as supplementary variables. These supplementary variables represented the spatial variability of seawater temperature, salinity, depth, dissolved oxygen, concentrations of total dissolved inorganic nitrogen, silicic acid and phosphate, DIC, TA, photosynthetically active radiation and fluorescence. The squared cosines of the variables were used to estimate the best link between each variable and the extracted principal component. Analyses were performed using the XLSTAT statistical package (version 2015.4.01.21575, Addinsoft).

3. Results and discussion

3.1. Overview of Hg speciation in the South Atlantic

THg (0.40–5.73 pmol L^{-1}), DGM (0.01–0.57 pmol L^{-1}) and MeHg concentrations (0.01–0.24 pmol L^{-1}) showed different distributions in the South Atlantic. Geometric means of THg and DGM concentrations in the South Atlantic were higher in the western part (1.42 and 0.18 pmol L^{-1}, respectively) compared to the eastern part (1.11 and 0.14 pmol L^{-1}, respectively), while MeHg values were the same (0.04 pmol L^{-1}; Fig. S2). THg did not show considerable vertical variation. MeHg was highest in the uppermost 200 m and lowest below 1000 m (geometric means 0.05 and 0.03 pmol L^{-1}, respectively). The geometric mean of the DGM concentration increased with depth from 0.08 pmol L^{-1} in the uppermost 200 m to 0.34 pmol L^{-1} at 1000 m, while the greatest values were found in the deepest waters (0.45 pmol L^{-1} below 4000 m; Fig. S2). Hg speciation was described in detail by Bratkič et al. (2016).

3.2. Correlations between DGM (MeHg) and environmental variables

The PCA was carried out on the data sets for Hg species. The analysis extracted two factors encompassing Hg species with similar patterns of spatial and vertical variabilities and explained 79% of the total variability. The first factor (D1) included high factor loading for DGM and MeHg and explained 44% of the variability. DGM was highly positively correlated with nutrients, DIC and depth, while MeHg was positively related with salinity, fluorescence and temperature. The second factor (D2) was considerably positively related with THg (the highest loading) and explained 35% of the variability. However, correlations with environmental variables were rather low (Fig. 1 and Table S1).

Positive correlations of DGM with DIC and nutrients (Table S2) might be due to microbial/abiotic Hg reduction during organic matter remineralization, as DGM and these variables generally all increase with depth (Fig. S2). Similarly, the observed significant negative correlation of DGM with temperature is due to corresponding temperature decrease with depth, as previously observed in the Central Adriatic Sea (Živković et al., 2019). On the contrary, MeHg generally has higher values in the mixed layer and in the warm surface waters where photosynthetically active radiation is the greatest. MeHg correlation with fluorescence/chlorophyll *a* indicates the possibility that Hg methylation is not linked only with organic matter degradation, but also with rapidly recycled fresh organic matter or that phototrophy may be (in)directly involved in Hg methylation (Bratkič et al., 2016).
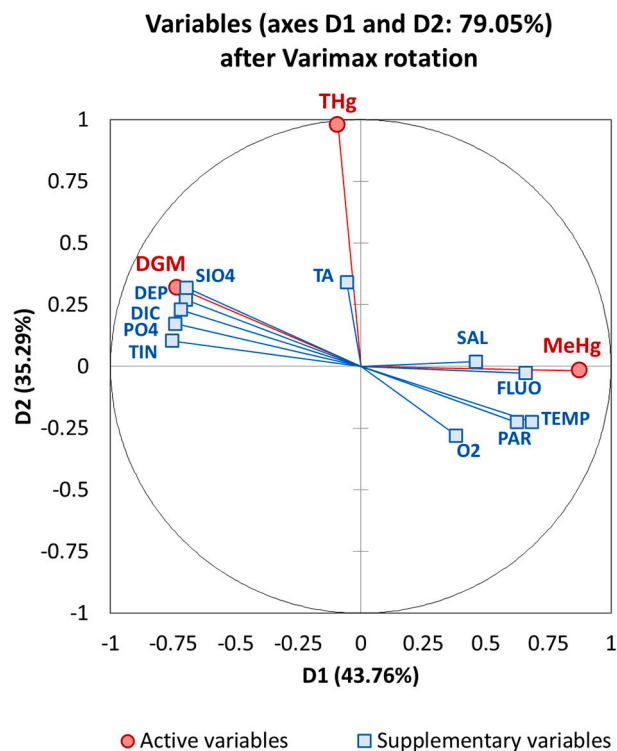

Variables (axes D1 and D2: 79.05%) after Varimax rotation

Fig. 1. Ordering of three Hg species as active variables obtained by the Principal Component Analysis along the South Atlantic transect. Abiotic variables are superimposed as supplementary variables and plotted as squares. Data used in graph (from Bratkič and Vahčič (2015) and Humphreys et al. (2016b)) are from eight stations along a 40°S transect and include 91 observations from surface to 4900 m depth. (Active variables: concentrations of total mercury, THg; dissolved gaseous mercury, DGM; methylated mercury, MeHg. Supplementary variables: total dissolved inorganic nitrogen, TIN; phosphate, PO4; silicic acid, SIO4; dissolved inorganic carbon, DIC; total alkalinity, TA; dissolved oxygen, O2; sea temperature, TEMP; ocean depth, DEP; salinity, SAL; photosynthetically active radiation, PAR; fluorescence, FLUO.)

3.3. Correlation between DGM and DIC

The reported concentration maximum of the dHg^0 in the North Atlantic Ocean indicated its formation by dark reactions at depth (Lamborg et al., 2021) and may have been related to organic matter remineralization (Bowman et al., 2015). Therefore, dHg^0 in deep water masses might be formed by either an abiotic or a microbial reduction process (Bowman et al., 2015). Most of the DGM in the deep South Atlantic waters is present as dHg^0, as DMeHg represents on average about 9% of DGM below 1000 m depth along 40°S (Bratkič and Vahčič, 2015). Microbial reduction of inorganic Hg^{II} is a possible pathway for DGM production in deep waters. Dissolution of settling particulate organic carbon (POC) and consequent DOC remineralization cause an increase in DIC concentrations in deep waters (Hupe et al., 2001). Even though several studies have demonstrated the effects of DOC concentration and quality on DGM (photo)production (Costa and Liss, 1999; Jiang et al., 2014; Zheng and Hintelmann, 2009), DIC might also be an appropriate proxy for DGM concentrations. However, direct comparison of DOC and DIC as proxies for DGM concentrations would be required to assess which one might be better.

DIC concentrations in the South Atlantic increased with depth until they reached an average value of 2231 μmol kg^{-1} between 1000 and 2000 m. Below this depth, DIC first decreased and then again increased towards the bottom (Fig. S3), which is related to the presence of different water masses (discussed in detail by Bratkič et al. (2016)). Therefore, DIC seems to be a better proxy for DGM than depth, as vertical profiles show peaks at about 1500 m (Figs. S2 and S3), and the corresponding correlations with depth are not linear.

To the best of our knowledge, this study is the first demonstration that DGM concentration increases linearly with increasing DIC concentration in the ocean (Fig. 2, Eq. (1)). This correlation indicates that either microbial/dark abiotic reductions produce DGM in deep waters, and/or that similar processes govern the behavior of DGM and DIC in seawater (e.g., similar processes in their respective solubility pumps or co-emission from active hydrothermal fluids in volcanic areas through diffuse degassing (Bagnato et al., 2018)).

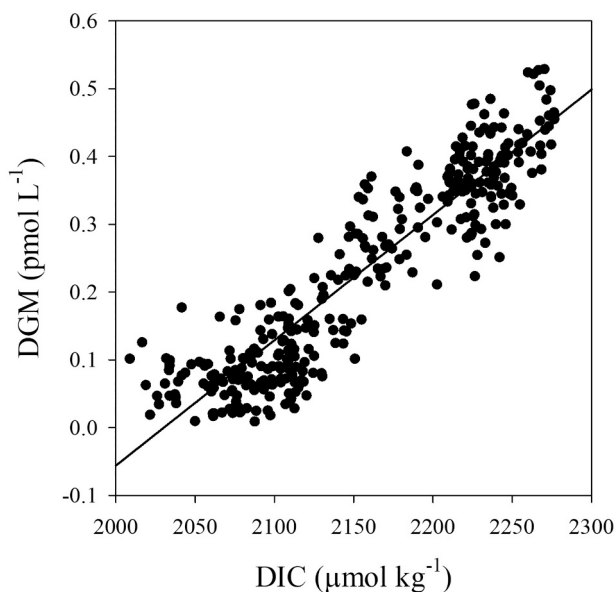There seems to exist a certain equivalence/similarity between Hg

Fig. 2. Linear correlation between dissolved inorganic carbon (DIC) and dissolved gaseous mercury (DGM) in South Atlantic waters ($r^2 = 0.844$). Units for DGM and DIC are those most commonly used in their respective literature. Data (from Bratkič and Vahčič (2015) and Humphreys et al. (2016b)) are from twenty stations along a 40°S transect and include 342 observations from surface to 5240 m depth (7 residual outliers were removed using the Dixon test).

reduction in seawater and in terrestrial soils. Hg^0 can be significantly correlated with CO_2 in soils (which are respective equivalents to marine dHg^0 and DIC). A fraction of Hg^0 may be emitted from soils to the atmosphere following reduction of Hg^{II} during carbon mineralization (Obrist et al., 2010), while the rest is emitted upon photoreduction of Hg^{II} (Costa and Liss, 1999). Therefore, the correlation between DGM and DIC found in the ocean water might be due to the in situ Hg^{II} reduction and not because of the solubility pump similar to that of CO_2.

$$DGM \left(pmol\ L^{-1}\right) = 0.00185\ kg\ L^{-1} \times DIC \left(\mu mol\ kg^{-1}\right) - 3.756\ pmol\ L^{-1}$$
(1)

Reduction of Hg^{II} during remineralization of organic matter as a probable explanation for the observed DGM–DIC relationship should be taken with reservations. Hydrothermal inputs could also explain the high DGM concentrations observed in deep waters. However, no DGM maxima were observed in the deepest layer (except at one station; Fig. S2). Also, there is a possibility that Hg^0 is bound to particulate matter (non-purgeable Hg^0), presumably due to high affinity of Hg^0 adsorption on solids (Wang et al., 2015), and might be released upon remineralization. Literature data also suggest that DMeHg can represent a larger fraction of the DGM in deep waters (Mason and Fitzgerald, 1993, 1990), contrary to what was found in this study. Demethylation of MeHg or DMeHg might present an additional pathway for dHg^0 production, as indicated by a negative correlation between DGM and MeHg (Table S2). This contribution might affect the linearity of DGM–DIC relationship and its use for the estimation of DGM concentrations in seawater.

3.4. Correlation between DGM and biological (remineralization) contribution to DIC

DIC is comprised of carbon originating from various sources (Sabine and Tanhua, 2010). To estimate how much DIC is derived from biological (remineralization) contributions without the effects of the solubility pump, preformed DIC needs to be subtracted (as described in Materials and Methods). DGM shows a significant correlation with remineralization contribution to DIC (DIC$_{bio}$; Fig. 3) indicating that carbon remineralization is possibly the driving force for the reduction of Hg^{II}.

$$DGM \left(pmol\ L^{-1}\right) = 0.00257\ kg\ L^{-1} \times DIC_{bio} \left(\mu mol\ kg^{-1}\right) + 0.0532\ pmol\ L^{-1}$$
(2)

The assessment of Hg reduction potential is usually estimated using DOC (DOM) concentrations. Schartup et al. (2015) showed that degradation of labile terrestrial organic matter reduces the stability of Hg bound to DOM, which enhances Hg^{II} reduction rates. DIC$_{bio}$ cannot explain any Hg-related transformations that might occur in seawater other than remineralization itself. As both DIC$_{bio}$ and possibly DGM are products of organic carbon remineralization, their use for describing Hg reduction in seawater might be more appropriate than comparing a reactant (DOM) and a product (DGM). Based on the slope of DIC$_{bio}$–DGM relationship (Eq. (2)), 390 μmol kg^{-1} of DOC has to be remineralized to DIC to create 1.0 pmol L^{-1} of DGM in seawater.

3.5. Testing equation on independent datasets

Independent datasets were used to test the robustness of Eq. (1) and the DGM–DIC relationship. DGM was calculated from DIC data from the Weddell Sea (Southern Ocean, near the Antarctic peninsula) (Wedborg et al., 1998) and compared with observed DGM values (Nerentorp Mastromonaco et al., 2017). Water column DIC values were uniform between 200 and 4000 m depth, and ranged from 2250 to 2260 μmol kg^{-1} at station 62 (locations of all discussed stations are provided in Table S3) (Wedborg et al., 1998). Using Eq. (1), DGM concentrations of 0.40–0.44 pmol L^{-1} can be calculated (Table S4). The average value
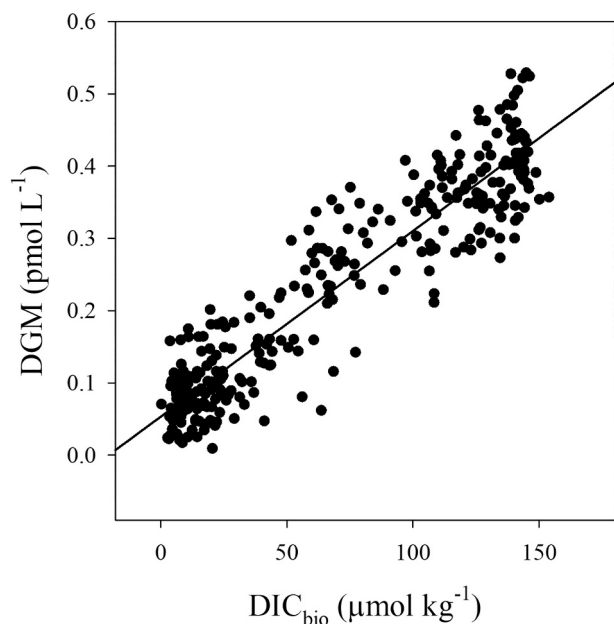
Fig. 3. Linear correlation between remineralization contribution to dissolved inorganic carbon (DIC$_{bio}$) and dissolved gaseous mercury (DGM) in South Atlantic waters ($r^2 = 0.871$). Units for DGM and DIC are those most commonly used in their respective literature. Data (from Bratkič and Vahčič (2015) and Humphreys et al. (2016b)) are from twenty stations along a 40°S transect and include 318 observations from surface to 5240 m depth (8 residual outliers were removed using Dixon test).

(0.42 ± 0.12 pmol L^{-1}) found at the nearby station 516–1 (Nerentorp Mastromonaco et al., 2017) falls within this range.

On the other hand, DGM results from the meridional cruise in the South and equatorial Atlantic Ocean (Mason and Sullivan, 1999) do not seem to follow Eq. (1) when compared to calculated DGM values from the data in the South Atlantic Ocean along 40°S. The average measured DGM concentration at station 10 (label from Mason and Sullivan (1999)) was 1.01 ± 0.36 pmol L^{-1}, which is significantly higher than calculated DGM values at the nearby stations 17 and 18 (label from current study, Fig. S1) (0.28 ± 0.14 pmol L^{-1}, Table S4) (Humphreys et al., 2016b). Nevertheless, these measured DGM and THg values were much higher than recent measurements along 40°S and in the Weddell Sea (Bratkič et al., 2016; Nerentorp Mastromonaco et al., 2017), indicating that other factors might also influence DGM production in these ecosystems. However, the most likely factor might be the analytical advance in Hg measurements.

DGM values calculated from DIC concentrations (Tilbrook et al., 2013) were also compared with directly measured concentrations in the Southern Ocean (DGM values were extracted from graphs) (Cossa et al., 2011). The ratio between the calculated and measured DGM values was on average 1.67 (17% RSD) below 1000 m depth (Table S5). MeHg profiles in the Southern Ocean indicate that DGM is mostly present as dHg^0 (Cossa et al., 2011), as in the South Atlantic. Therefore, methylated mercury should probably not be included into DGM when considering correlation with DIC, as dHg^0 contributes to the majority of DGM. However, DGM is a method-dependent Hg fraction and it cannot be separated into constituent species.

In addition to the relatively constant ratio between DGM and DIC in deep ocean waters, the greatest DGM peak observed at 100 m depth (0.59 pmol L^{-1}) (Cossa et al., 2011) at station N-04 coincides with an extremely elevated (though discarded) DIC concentration (4384 μmol kg^{-1}) (Tilbrook et al., 2013). However, the DGM–DIC relationship at this station does not follow Eq. (1), possibly due to greater DGM degassing to the atmosphere from the upper ocean (greater concentration gradient) or more probably, due to a real error during DIC determination. Further

issues can arise from different experimental procedures for the determination of DGM in seawater.

3.6. Testing equation on independent datasets using modeled DIC values

As the availability of DIC data simultaneously determined alongside DGM measurements are scarce, we also used modeled DIC data. Modeled DIC values from Goyet et al. (2000a, 2000b) were previously determined at 1° × 1° resolution from surface to bottom waters for world oceans between 66.5° N and 66.5° S. Calculated DGM concentrations were determined by applying our obtained DGM–DIC relationship (Eq. (1)) to these values. Measured DGM values from the Mediterranean Sea (data from two oceanographic cruises from Kotnik et al. (2007) and unpublished data from two oceanographic cruises during 2015 and 2017) were compared with geographically closest calculated DGM concentrations. Calculated and measured DGM values were in a good agreement (Fig. 4; all four aforementioned cruises), especially below 1500 m depth where calculated DGM values were within ±25% of the measured DGM values. The exceptions were usually surface values (due to photochemical reduction (Monperrus et al., 2007); Fig. 4E, F and H) and bottom values (due to tectonic activity (Kotnik et al., 2007); Fig. 4L). DGM determined at coastal sites were left out from this analysis as the comparison with calculated DGM at the nearest point at 1° × 1° resolution almost never gave comparable results (not shown), probably because Eq. (1) was derived from open ocean measurements. The greatest discrepancies between calculated and measured DGM values were between the photic layer and 1000 m where DIC concentrations rapidly increase with depth (Fig. S3). This indicates that DGM–DIC relationship obtained from the South Atlantic might not be the same in all waters. However, all models that depend on profiles of DIC, nutrients, and other physical parameters suffer from uncertainties and model-model/model-data disagreements between each other (Key et al., 2004; Murnane et al., 1999; Séférian et al., 2013).

The increase in DIC and associated increase in DGM are the result of a combination of increases in anthropogenic CO_2/Hg taken up by the ocean and distributed through the solubility pump (currently mainly in younger water masses), and increases in organic matter remineralization related to sinking particles (vertical increase) or water mass movement (horizontal changes)/changes in the amount of sinking particles. However, the ratio of CO_2 to Hg in younger water masses is probably not constant due to different anthropogenic burdens. To eliminate these differences in respective solubility pumps, we tested whether DGM might be related only with organic matter remineralization in the upper 1000 m. Because of discrepancies between calculated and measured DGM values, we tested whether the DGM–DIC$_{bio}$ relationship yielded better results. To test whether DGM might be related to organic matter remineralization we calculated DIC$_{bio}$ from the available dataset (Goyet et al., 2000b), while the corresponding DGM was determined using the DGM–DIC$_{bio}$ relation (Eq. (2)) in the upper 1000 m. As this available dataset and DIC$_{bio}$ are themselves modeled, DGM calculated using this approach is directly dependent only on four variables: pressure, water temperature, salinity, and oxygen concentration.

Comparison of calculated and measured DGM concentrations (Fig. 5) showed much better agreement than when using the DGM–DIC relationship. Calculated DGM differed from the measured DGM by 13% (geometric mean) between 150 and 1000 m depth. A station in the Strait of Sicily (ST4) was not taken into an account due to probably elevated concentrations of preformed DGM (strong tectonic and volcanic activity) (Kotnik et al., 2007). The analysis was performed only for depths down to 1000 m, because in the model for the calculation of total alkalinity (Goyet et al., 2000b), the water column was divided into two separate zones: from the bottom of the wintertime mixed layer down to 1000 m and from 1000 m to the bottom. In the Mediterranean Sea, this caused an abrupt rise in total alkalinity at 1000 m and consequently corresponding rise in calculated DGM values (not shown) that were several times greater than the observations.
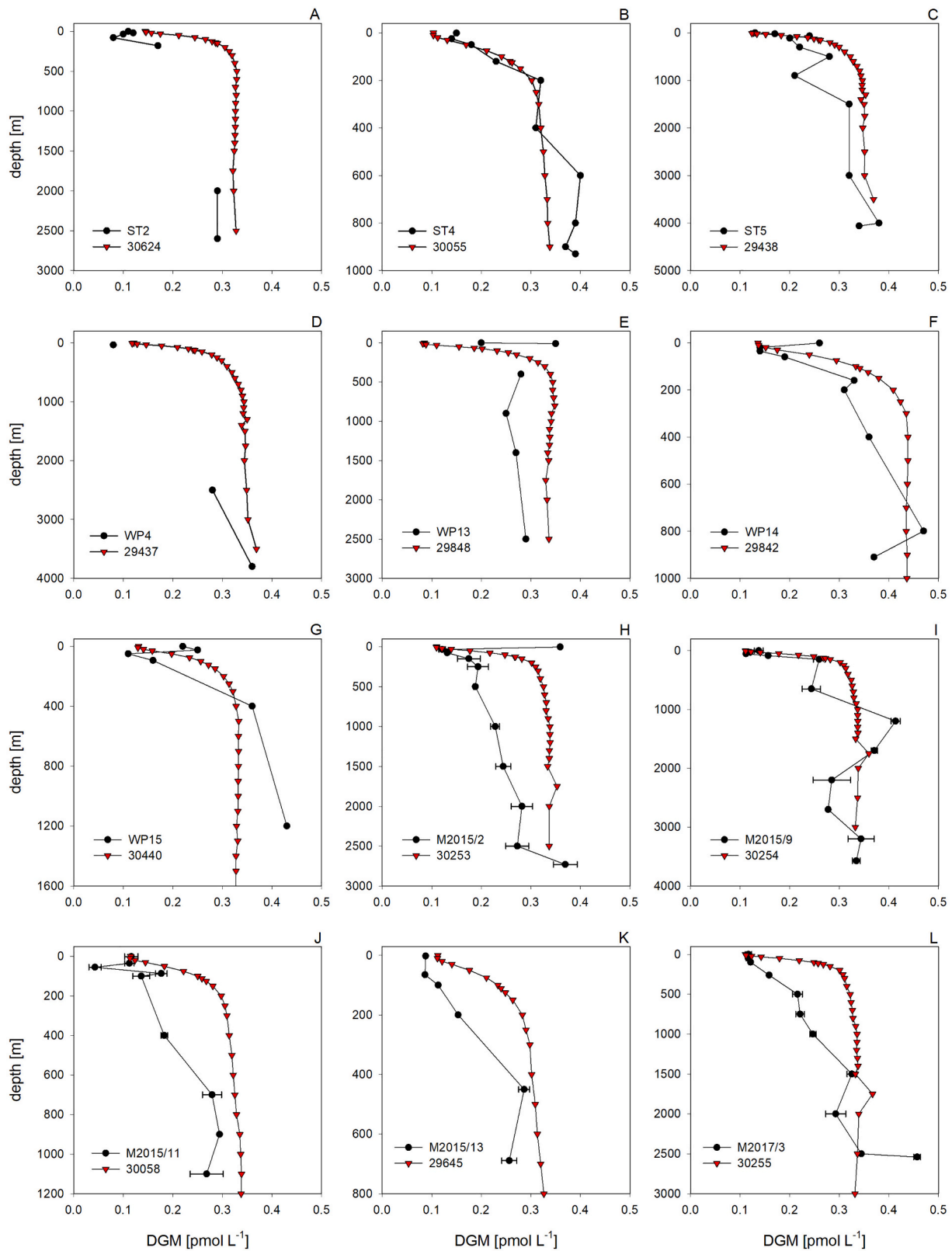
Fig. 4. Comparison of vertical profiles of DGM measured in the Mediterranean Sea (data from Kotnik et al. (2007) and two oceanographic cruises during 2015 and 2017; black circles) with DGM values calculated using Eq. (1): DIC–DGM relationship (DIC data from Goyet et al., 2000b; red triangles). Sampling point locations are presented in Table S3. Error bars represent one standard deviation of parallel measurements (where available). Gaps between black circles are due to excluded data in the original publication. (For interpretation of the references to colour in this figure legend, the reader is referred to the web version of this article.)
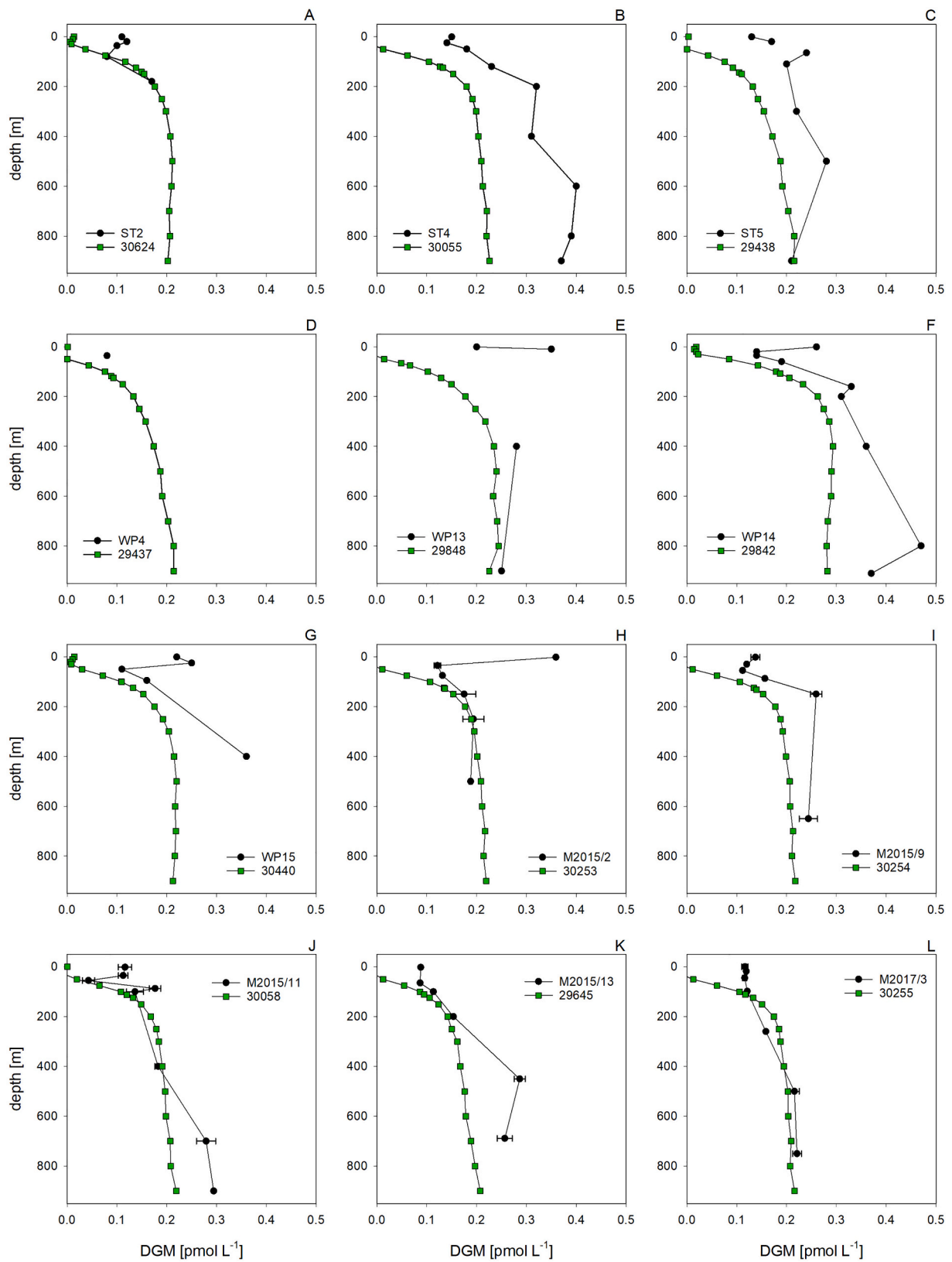
Fig. 5. Comparison of vertical profiles of DGM (upper 1000 m) measured in the Mediterranean Sea (data from Kotnik et al. (2007) and two oceanographic cruises during 2015 and 2017; black circles) with calculated DGM values using Eq. (2): DIC$_{bio}$–DGM relation (data from Goyet et al. (2000b); green squares). Sampling point locations are presented in Table S3. Error bars represent one standard deviation of parallel measurements (where available). Gaps between black circles are due to excluded data in the original publication. (For interpretation of the references to colour in this figure legend, the reader is referred to the web version of this article.)

Furthermore, calculated DIC_{bio} is influenced by modeled values of preformed total alkalinity, TA^0. This variable strongly depends on potential temperature θ and available models show errors in TA^0 in cold deep waters ($\theta < 5$ °C). This is probably another reason for the disagreement between model and DGM observations in deep waters. Due to these reasons, we calculated DGM using the DGM–DIC_{bio} relationship only in the upper 1000 m and using DGM–DIC relation in deep waters.

It is also necessary to emphasize that the DGM–DIC_{bio} correlation (Eq. (2)) was constructed using data from the entire water column because the obtained p value (<0.001) was much lower than the p value (0.047) obtained for the corresponding equation constructed using data only from the upper 1000 m. Nevertheless, the differences between DGM values calculated using these two equations were marginal (range from -0.2% to 0.5%, with an average of 0.12%). As these differences were insignificant compared to differences between modeled and measured DGM values, we opted for the use of Eq. (2).

The DGM–DIC_{bio} relationship was also tested in the Northwestern Pacific Ocean, where higher DGM concentrations (> 0.5 pmol L^{-1}) can be found compared to the South Atlantic Ocean. These values were not used for the determination of the DGM–DIC_{bio} relationship and the corresponding DIC_{bio} values are out of the used range (0–150 μmol kg^{-1}; Fig. 3). Nevertheless, good agreement was obtained when comparing measured DGM concentrations (H. Kim et al., 2016) with calculated DGM from modeled DIC_{bio} data (Goyet et al., 2000b) (Fig. S4). Calculated DGM differed from the measured DGM by 14% (geometric mean) between 100 and 500 m depth (not taking into account station K4).

Calculated DGM concentrations in a zonal section across the North Atlantic Ocean (GEOTRACES GA03 cruise) (Bowman et al., 2015; Lamborg and Hammerschmidt, 2017) yielded contradictory results between the eastern and western parts. The DGM–DIC_{bio} relationship yielded comparable DGM values (characteristic subsurface maximum of about 0.5 pmol L^{-1} between 200 and 1000 m; Fig. S5) with measured values (sum of dHg^0 and DMeHg) in the eastern part of the zonal section. This confirms the hypothesis that higher DGM concentrations are related to dark reactions in oxygen deficient zone and coincident with organic matter remineralization (Bowman et al., 2015). DGM in deep waters (about 0.3 pmol L^{-1}), calculated using the DGM–DIC relationship, also agreed well with measured values in the eastern part. However, measured and calculated DGM disagreed in deep waters of the western part, where measured values were two to three-fold higher than calculated ones. The hypothesis that higher dHg^0 and DMeHg concentrations in the western part are due to greater Hg substrate availability or greater methylation and reduction potentials in younger deep waters (Bowman et al., 2015) casts questions about robustness of using the DGM–DIC relationship to predict DGM concentrations. It is possible that demethylation of methylated Hg species (Whalin et al., 2007) might represent additional pathway of dHg^0 production in these waters containing elevated DMeHg concentrations (Cossa et al., 1994). This might explain why DGM (dHg^0) produced by reduction during organic carbon remineralization do not match observations. Furthermore, the solubility pump may potentially move Hg into these young waters, together with anthropogenic CO_2. However, the ratio of CO_2 and Hg in these waters is probably not the same as in older waters due to anthropogenic burdens, which could be the cause of the observed differences.

3.7. Estimation of DGM concentrations from nutrients

Including additional variables besides DIC might provide better estimates of DGM concentrations. Using multiple linear regression analysis, DGM concentrations were estimated from various environmental variables, mainly nutrients. TIN (Fig. S3) was identified as the most appropriate variable due to the lowest variance inflation factor. The chosen multiple linear regression (Eq. (3)) had the highest correlation coefficient ($R^2 = 0.855$) among investigated variables.

$$\begin{aligned} DGM \; (\text{pmol } L^{-1}) = {} & 0.00122 \text{ kg } L^{-1} \times DIC \; (\mu\text{mol kg}^{-1}) \\ & + 0.00365 \times TIN \; (\mu\text{mol } L^{-1}) - 2.472 \text{ pmol } L^{-1} \end{aligned} \quad (3)$$

Using this equation, DGM can be estimated within $\pm20\%$ of the measured value in 50% of the whole dataset. Assuming the predominance of photochemical reactions on Hg reduction in the surface ocean waters (Qureshi et al., 2010) over biotic and abiotic reactions, we took into consideration only values obtained below 200 m. Eq. (3) can estimate DGM within $\pm20\%$ of the measured value in 74% of the data below 200 m and in 80% of the data below 400 m. This demonstrates the different behavior of Hg and DIC in surface waters where photoreduction of Hg plays an important role. Therefore, Eq. (3) could be used for the estimation of DGM concentrations in deep waters.

Bowman et al. (2015) observed an unexpected nutrient-type vertical profile of dHg^0 in the North Atlantic Ocean that had not been previously documented. Bratkič et al. (2016) found the same relationship between DGM and nitrate in South Atlantic waters (using the same dataset as in this study; Figs. S2 and S3). Because of the observed correlations between DGM and both DIC and TIN, we agree that DGM production might be related to organic matter remineralization and deep water dark abiotic reactions (Jiang et al., 2014; Oh et al., 2011). Decomposition of organic matter to DIC and TIN might generate a reducing potential in anoxic microenvironments of sinking particles (Bianchi et al., 2018) great enough for the reduction of inorganic Hg.

4. Conclusions

This study demonstrated that DGM concentrations might be calculated based on DIC and/or nutrients data. Our assessment of DGM values is intended as a proof-of-concept that other variables might be used as proxies for global Hg concentrations. The DGM values obtained either using empirical DGM–DIC or DGM–DIC_{bio} relationships mostly agreed with the observations, even when used DIC values are modeled themselves. Based on our results, we presume that DGM production was controlled photochemically in the surface layer, might be associated with the remineralization of labile organic matter down to about 1000 m depth, and the remineralization of refractory organic matter in the deepest waters (related to the highest DIC values). Our results suggests that DIC might be used as a proxy for DGM, possibly as a consequence of organic matter remineralization. Future research should experimentally test whether the DGM–DIC correlation found in the South Atlantic Ocean is present in other ocean basins. If confirmed, this relationship could have significant implications for Hg models in open ocean waters.

CRediT authorship contribution statement

Igor Živković: Conceptualization, Data curation, Investigation, Formal analysis, Methodology, Validation, Visualization, Writing – original draft. **Matthew P. Humphreys:** Data curation, Formal analysis, Methodology, Resources, Software, Validation, Writing – original draft. **Eric P. Achterberg:** Conceptualization, Funding acquisition, Investigation, Data curation, Methodology, Project administration, Supervision, Validation, Writing – original draft. **Cynthia Dumousseaud:** Data curation, Formal analysis, Methodology, Validation, Writing – original draft. **E. Malcolm S. Woodward:** Formal analysis, Methodology, Resources, Validation, Writing – review & editing. **Natalia Bojanić:** Formal analysis, Investigation, Methodology, Validation, Writing – review & editing. **Mladen Šolić:** Formal analysis, Funding acquisition, Investigation, Methodology, Project administration, Resources, Writing – review & editing. **Arne Bratkič:** Data curation, Formal analysis, Investigation, Methodology, Writing – review & editing. **Jože Kotnik:** Data curation, Formal analysis, Investigation, Methodology, Validation, Writing – review & editing. **Mitja Vahčič:** Data curation, Formal analysis, Methodology, Validation, Writing – review & editing. **Kristina Obu Vazner:** Data curation, Formal analysis, Methodology, Validation,

Appendix A. Supplementary data

Supplementary data to this article can be found online at https://doi.org/10.1016/j.marpolbul.2022.113644.

References

Amos, H.M., Jacob, D.J., Streets, D.G., Sunderland, E.M., 2013. Legacy impacts of all-time anthropogenic emissions on the global mercury cycle. Glob. Biogeochem. Cycles 27, 410–421. https://doi.org/10.1002/gbc.20040.

Andersson, M.E., Gårdfeldt, K., Wängberg, I., Strömberg, D., 2008. Determination of Henry's law constant for elemental mercury. Chemosphere 73, 587–592. https://doi.org/10.1016/j.chemosphere.2008.05.067.

Bach, L.T., Stange, P., Taucher, J., Achterberg, E.P., Alguero-Muñiz, M., Horn, H., Esposito, M., Riebesell, U., 2019. The influence of plankton community structure on sinking velocity and remineralization rate of marine aggregates. Glob. Biogeochem. Cycles 33, 971–994. https://doi.org/10.1029/2019GB006256.

Bagnato, E., Viveiros, F., Pacheco, J.E., D'Agostino, F., Silva, C., Zanon, V., 2018. Hg and CO2 emissions from soil diffuse degassing and fumaroles at furnas volcano (São Miguel Island, Azores): gas flux and thermal energy output. J. Geochem. Explor. 190, 39–57. https://doi.org/10.1016/j.gexplo.2018.02.017.

Bianchi, D., Weber, T.S., Kiko, R., Deutsch, C., 2018. Global niche of marine anaerobic metabolisms expanded by particle microenvironments. Nat. Geosci. 11, 263–268. https://doi.org/10.1038/s41561-018-0081-0.

Bowman, K.L., Hammerschmidt, C.R., Lamborg, C.H., Swarr, G., 2015. Mercury in the North Atlantic Ocean: the U.S. GEOTRACES zonal and meridional sections. DeepRes. Part II Top. Stud. Oceanogr. 116, 251–261. https://doi.org/10.1016/j.dsr2.2014.07.004.

Bratkič, A., Vahčič, M., 2015. Concentrations of Various Mercury Species (Total Mercury, THg; Monomethyl Mercury, MeHg; Dissolved Gaseous Mercury, DGM; and Dimethylmercury, DMeHg) as Measured During GA10 GEOTRACES Cruise in the South Atlantic Ocean. British Oceanographic Data Centre - Natural Environment Research Council. https://doi.org/10.5285/1dbc9294-4e65-6530-e053-6c86abc09fb2. (Accessed 15 January 2019).

Bratkič, A., Vahčič, M., Kotnik, J., Obu Vazner, K., Begu, E., Woodward, E.M.S., Horvat, M., 2016. Mercury presence and speciation in the South Atlantic Ocean along the 40°S transect. Glob. Biogeochem. Cycles 30, 105–119. https://doi.org/10.1002/2015GB005275.

Chen, Y.-S., Tseng, C.-M., Reinfelder, J.R., 2020. Spatiotemporal variations in dissolved elemental mercury in the river-dominated and monsoon-influenced East China Sea: drivers, budgets, and implications. Environ. Sci. Technol. 54, 3988–3995. https://doi.org/10.1021/acs.est.9b06092.

Compeau, G.C., Bartha, R., 1987. Effect of salinity on mercury-methylating activity of sulfate-reducing bacteria in estuarine sediments. Appl. Environ. Microbiol. 53, 261–265.

Cossa, D., Averty, B., Pirrone, N., 2009. The origin of methylmercury in open mediterranean waters. Limnol. Oceanogr. 54, 837–844. https://doi.org/10.4319/lo.2009.54.3.0837.

Cossa, D., Heimbürger, L.E., Lannuzel, D., Rintoul, S.R., Butler, E.C.V., Bowie, A.R., Averty, B., Watson, R.J., Remenyi, T., 2011. Mercury in the Southern Ocean. Geochim. Cosmochim. Acta 75, 4037–4052. https://doi.org/10.1016/j.gca.2011.05.001.

Cossa, D., Martin, J.-M., Sanjuan, J., 1994. Dimethylmercury formation in the Alboran Sea. Mar. Pollut. Bull. 28, 381–384. https://doi.org/10.1016/0025-326X(94)90276-3.

Costa, M., Liss, P.S., 1999. Photoreduction of mercury in sea water and its possible implications for Hg0 air-sea fluxes. Mar. Chem. 68, 87–95. https://doi.org/10.1016/S0304-4203(99)00067-5.

Fantozzi, L., Ferrara, R., Frontini, F.P., Dini, F., 2009. Dissolved gaseous mercury production in the dark: evidence for the fundamental role of bacteria in different types of Mediterranean water bodies. Sci. Total Environ. 407, 917–924. https://doi.org/10.1016/j.scitotenv.2008.09.014.

Garcia, H.E., Gordon, L.I., 1992. Oxygen solubility in seawater: better fitting equations. Limnol. Oceanogr. 37, 1307–1312. https://doi.org/10.4319/lo.1992.37.6.1307.

Gårdfeldt, K., Sommar, J., Ferrara, R., Ceccarini, C., Lanzillotta, E., Munthe, J., Wängberg, I., Lindqvist, O., Pirrone, N., Sprovieri, F., Pesenti, E., Strömberg, D., 2003. Evasion of mercury from coastal and open waters of the Atlantic Ocean and the Mediterranean Sea. Atmos. Environ. 37, 73–84. https://doi.org/10.1016/S1352-2310(03)00238-3.

Giering, S.L.C., Humphreys, M.P., 2017. Biological pump. In: White, W. (Ed.), Encyclopedia of Geochemistry, Encyclopedia of Earth Sciences Series. Springer, Cham, Switzerland, pp. 1–6. https://doi.org/10.1007/978-3-319-39193-9_154-1.

Goyet, C., Healy, R., Ryan, J., Kozyr, A., 2000. Global Alkalinity and Total Dissolved Carbon Estimates. https://odv.awi.de/data/ocean/global-alkanity-tco2/. (Accessed 15 March 2020).

Goyet, C., Healy, R., Ryan, J., Kozyr, A., 2000. Global Distribution of Total Inorganic Carbon and Total Alkalinity below the Deepest Winter Mixed Layer Depths. Oak Ridge National Laboratory, Oak Ridge, US. https://doi.org/10.2172/760546.

Grégoire, D.S., Poulain, A.J., 2016. A physiological role for HgII during phototrophic growth. Nat. Geosci. 9, 121–125. https://doi.org/10.1038/ngeo2629.

Grégoire, D.S., Poulain, A.J., 2014. A little bit of light goes a long way: the role of phototrophs on mercury cycling. Metallomics 6, 396. https://doi.org/10.1039/c3mt00312d.

Gu, B., Bian, Y., Miller, C.L., Dong, W., Jiang, X., Liang, L., 2011. Mercury reduction and complexation by natural organic matter in anoxic environments. Proc. Natl. Acad. Sci. 108, 1479–1483. https://doi.org/10.1073/pnas.1008747108.

Hansell, D.A., Carlson, C.A. (Eds.), 2015. Biogeochemistry of Marine Dissolved Organic Matter, 2nd ed. Elsevier, London, UK. https://doi.org/10.1016/C2012-0-02714-7.

Heimbürger, L.E., Cossa, D., Marty, J.C., Migon, C., Averty, B., Dufour, A., Ras, J., 2010. Methyl mercury distributions in relation to the presence of nano- and picophytoplankton in an oceanic water column (Ligurian Sea, North-Western Mediterranean). Geochim. Cosmochim. Acta 74, 5549–5559. https://doi.org/10.1016/j.gca.2010.06.036.

Humphreys, M.P., 2015. Calculating seawater total alkalinity from open-cell titration data using a modified Gran plot technique. In: Measurements and Concepts in Marine Carbonate Chemistry. University of Southampton, Southampton, UK, pp. 25–44.

Humphreys, M.P., Dumousseaud, C., Achterberg, E.P., 2016. GA10 Carbonate Chemistry. GEOTRACES Standards & Intercalibration Committee. https://doi.org/10.13140/RG.2.1.1394.3926.

Humphreys, M.P., Dumousseaud, C., Achterberg, E.P., 2016. Discrete Carbonate Chemistry Measurements From UK GEOTRACES Cruises D357 and JC068 on the South Atlantic Transect GA10. British Oceanographic Data Centre - Natural Environment Research Council. https://doi.org/10.5285/33d2c2c7-84dc-718b-e053-6c86abc0da4d. (Accessed 15 January 2020).

Humphreys, M.P., Griffiths, A.M., Achterberg, E.P., Holliday, N.P., Rérolle, V.M.C., Menzel Barraqueta, J.-L., Couldrey, M.P., Oliver, K.I.C., Hartman, S.E., Esposito, M., Boyce, A.J., 2016c. Multidecadal accumulation of anthropogenic and remineralized dissolved inorganic carbon along the extended ellett line in the Northeast Atlantic Ocean. Glob. Biogeochem. Cycles 30, 293–310. https://doi.org/10.1002/2015GB005246.

Hupe, A., Thomas, H., Ittekkot, V., Lendt, R., 2001. Inventory of released inorganic carbon from organic matter remineralization in the deeper Arabian Sea. J. Geophys. Res. Ocean. 106, 31189–31196. https://doi.org/10.1029/2000jc000427.

Jiang, T., Wei, S.-Q., Flanagan, D.C., Li, M.-J., Li, X.-M., Wang, Q., Luo, C., 2014. Effect of abiotic factors on the mercury reduction process by humic acids in aqueous systems. Pedosphere 24, 125–136. https://doi.org/10.1016/S1002-0160(13)60087-9.

Joshi, D., Meena, B., Verma, P., Nayak, J., Vinithkumar, N.V., Dharani, G., 2021. Deep-sea mercury resistant bacteria from the Central Indian Ocean: a potential candidate for mercury bioremediation. Mar. Pollut. Bull. 169, 112549 https://doi.org/10.1016/j.marpolbul.2021.112549.

Key, R.M., Kozyr, A., Sabine, C.L., Lee, K., Wanninkhof, R., Bullister, J.L., Feely, R.A., Millero, F.J., Mordy, C., Peng, T.-H., 2004. A global ocean carbon climatology: results from global data analysis project (GLODAP). Glob. Biogeochem. Cycles 18, GB4031. https://doi.org/10.1029/2004GB002247.

Kim, H., Rhee, T.S., Hahm, D., Hwang, C.Y., Yang, J., Han, S., 2016. Contrasting distributions of dissolved gaseous mercury concentration and evasion in the North Pacific subarctic gyre and the subarctic front. Deep Sea resPart I Oceanogr. Res. Pap. 110, 90–98. https://doi.org/10.1016/j.dsr.2016.02.001.

Kim, M.-K., Won, A.-Y., Zoh, K.-D., 2016. The production of dissolved gaseous mercury from methylmercury photodegradation at different salinity. Desalin. Water Treat. 57, 610–619. https://doi.org/10.1080/19443994.2014.986829.

Körtzinger, A., Quay, P.D., Sonnerup, R.E., 2003. Relationship between anthropogenic CO2 and the 13C suess effect in the North Atlantic Ocean. Glob. Biogeochem. Cycles 17, 1–20. https://doi.org/10.1029/2001GB001427.

Kotnik, J., Horvat, M., Tessier, E., Ogrinc, N., Monperrus, M., Amouroux, D., Fajon, V., Gibičar, D., Žižek, S., Sprovieri, F., Pirrone, N., 2007. Mercury speciation in surface and deep waters of the Mediterranean Sea. Mar. Chem. 107, 13–30. https://doi.org/10.1016/j.marchem.2007.02.012.

Lamborg, C.H., Hammerschmidt, C., 2017. Mercury Speciation Across the US GEOTRACES North Atlantic Zonal Section From R/V Knorr KN199-04, KN204-01 in the Subtropical North Atlantic Ocean From 2010-2011 (U.S. GEOTRACES NAT Project). Biological and Chemical Oceanography Data Management Office (BCO-DMO). https://www.bco-dmo.org/dataset/3860/data. (Accessed 15 March 2020).

Lamborg, C.H., Hansel, C.M., Bowman, K.L., Voelker, B.M., Marsico, R.M., Oldham, V.E., Swarr, G.J., Zhang, T., Ganguli, P.M., 2021. Dark reduction drives evasion of mercury from the ocean. Front. Environ. Chem. 2, 1–16. https://doi.org/10.3389/fenvc.2021.659085.

Lea, D.W., 2014. Elemental and isotopic proxies of past ocean temperatures. In: Treatise on Geochemistry. Elsevier, pp. 373–397. https://doi.org/10.1016/B978-0-08-095975-7.00614-8.

Mason, R.P., Fitzgerald, W.F., 1993. The distribution and biogeochemical cycling of mercury in the equatorial Pacific Ocean. Deep Sea resPart I Oceanogr. Res. Pap. 40, 1897–1924. https://doi.org/10.1016/0967-0637(93)90037-4.

Mason, R.P., Fitzgerald, W.F., 1990. Alkylmercury species in the equatorial Pacific. Nature 347, 457–459. https://doi.org/10.1038/347457a0.

Mason, R.P., Fitzgerald, W.F., Morel, F.M.M., 1994. The biogeochemical cycling of elemental mercury: anthropogenic influences. Geochim. Cosmochim. Acta 58, 3191–3198. https://doi.org/10.1016/0016-7037(94)90046-9.

Mason, R.P., Sullivan, K.A., 1999. The distribution and speciation of mercury in the south and equatorial Atlantic. DeepRes. Part II Top. Stud. Oceanogr. 46, 937–956. https://doi.org/10.1016/S0967-0645(99)00010-7.

Matsuyama, A., Yano, S., Taniguchi, Y., Kindaichi, M., Tada, A., Wada, M., 2021. Trends in mercury concentrations and methylation in Minamata Bay, Japan, between 2014 and 2018. Mar. Pollut. Bull. 173, 112886 https://doi.org/10.1016/j.marpolbul.2021.112886.

Monperrus, M., Tessier, E., Amouroux, D., Leynaert, A., Huonnic, P., Donard, O.F.X., 2007. Mercury methylation, demethylation and reduction rates in coastal and marine surface waters of the Mediterranean Sea. Mar. Chem. 107, 49–63. https://doi.org/10.1016/j.marchem.2007.01.018.

Murnane, R.J., Sarmiento, J.L., Le Quéré, C., 1999. Spatial distribution of air-sea CO2 fluxes and the interhemispheric transport of carbon by the oceans. Glob. Biogeochem. Cycles 13, 287–305. https://doi.org/10.1029/1998GB900009.

Nerentorp Mastromonaco, M.G., Gårdfeldt, K., Assmann, K.M., Langer, S., Delali, T., Shlyapnikov, Y.M., Zivkovic, I., Horvat, M., 2017. Speciation of mercury in the waters of the weddell, Amundsen and Ross seas (Southern Ocean). Mar. Chem. 193, 20–33. https://doi.org/10.1016/j.marchem.2017.03.001.

Obrist, D., Faïn, X., Berger, C., 2010. Gaseous elemental mercury emissions and CO2 respiration rates in terrestrial soils under controlled aerobic and anaerobic laboratory conditions. Sci. Total Environ. 408, 1691–1700. https://doi.org/10.1016/j.scitotenv.2009.12.008.

Oh, S., Kim, M.K., Lee, Y.M., Zoh, K.D., 2011. Effect of abiotic and biotic factors on the photo-induced production of dissolved gaseous mercury. Water Air Soil Pollut. 220, 353–363. https://doi.org/10.1007/s11270-011-0759-z.

Poulain, A.J., Amyot, M., Findlay, D., Telor, S., Barkay, T., Hintelmann, H., 2004. Biological and photochemical production of dissolved gaseous mercury in a boreal lake. Limnol. Oceanogr. 49, 2265–2275. https://doi.org/10.4319/lo.2004.49.6.2265.

Qureshi, A., O'Driscoll, N.J., MacLeod, M., Neuhold, Y.-M., Hungerbühler, K., 2010. Photoreactions of mercury in Surface Ocean water: gross reaction kinetics and possible pathways. Environ. Sci. Technol. 44, 644–649. https://doi.org/10.1021/es9012728.

Sabine, C.L., Tanhua, T., 2010. Estimation of anthropogenic CO2 inventories in the ocean. Annu. Rev. Mar. Sci. 2, 175–198. https://doi.org/10.1146/annurev-marine-120308-080947.

Schartup, A.T., Ndu, U., Balcom, P.H., Mason, R.P., Sunderland, E.M., 2015. Contrasting effects of marine and terrestrially derived dissolved organic matter on mercury speciation and bioavailability in seawater. Environ. Sci. Technol. 49, 5965–5972. https://doi.org/10.1021/es506274x.

Séférian, R., Bopp, L., Gehlen, M., Orr, J.C., Ethé, C., Cadule, P., Aumont, O., Salas Mélia, D., Voldoire, A., Madec, G., 2013. Skill assessment of three earth system models with common marine biogeochemistry. Clim. Dyn. 40, 2549–2573. https://doi.org/10.1007/s00382-012-1362-8.

Slemr, F., Brunke, E.-G., Ebinghaus, R., Temme, C., Munthe, J., Wängberg, I., Schroeder, W., Steffen, A., Berg, T., 2003. Worldwide trend of atmospheric mercury since 1977. Geophys. Res. Lett. 30, 23. https://doi.org/10.1029/2003GL016954.

Strode, S., Jaeglé, L., Emerson, S., 2010. Vertical transport of anthropogenic mercury in the ocean. Glob. Biogeochem. Cycles 24, GB4014. https://doi.org/10.1029/2009GB003728.

Sunderland, E.M., Krabbenhoft, D.P., Moreau, J.W., Strode, S.A., Landing, W.M., 2009. Mercury sources, distribution, and bioavailability in the North Pacific Ocean: insights from data and models. Glob. Biogeochem. Cycles 23, 1–14. https://doi.org/10.1029/2008GB003425.

Sunderland, E.M., Mason, R.P., 2007. Human impacts on open ocean mercury concentrations. Glob. Biogeochem. Cycles 21, GB4022. https://doi.org/10.1029/2006GB002876.

Tilbrook, B., Rintoul, S.R., Warner, M.J., Hansell, D.A., Rosenberg, M., 2013. Dissolved Inorganic Carbon (DIC), Total Alkalinity, Temperature, Salinity and Other Variables Collected From Discrete Sample and Profile Observations During the R/V Aurora Australis Cruise AU0806, CLIVAR_SR03_2008 (EXPOCODE 09AR20080322) in the Indian Ocean From 2008-03-22 to 2008-04-17. NOAA National Centers for Environmental Information. https://doi.org/10.3334/cdiac/otg.clivar_sr03_2008. (Accessed 15 March 2019).

Wang, Y., Li, Y., Liu, G., Wang, D., Jiang, G., Cai, Y., 2015. Elemental mercury in natural waters: occurrence and determination of particulate Hg(0). Environ. Sci. Technol. 49, 9742–9749. https://doi.org/10.1021/acs.est.5b01940.

Wedborg, M., Hoppema, M., Skoog, A., 1998. On the relation between organic and inorganic carbon in the Weddell Sea. J. Mar. Syst. 17, 59–76. https://doi.org/10.1016/S0924-7963(98)00029-3.

Whalin, L., Kim, E.-H., Mason, R., 2007. Factors influencing the oxidation, reduction, methylation and demethylation of mercury species in coastal waters. Mar. Chem. 107, 278–294. https://doi.org/10.1016/j.marchem.2007.04.002.

Zheng, W., Hintelmann, H., 2010. Nuclear field shift effect in isotope fractionation of mercury during abiotic reduction in the absence of light. J. Phys. Chem. A 114, 4238–4245. https://doi.org/10.1021/jp910353y.

Zheng, W., Hintelmann, H., 2009. Mercury isotope fractionation during photoreduction in natural water is controlled by its Hg/DOC ratio. Geochim. Cosmochim. Acta 73, 6704–6715. https://doi.org/10.1016/j.gca.2009.08.016.

Zheng, W., Liang, L., Gu, B., 2012. Mercury reduction and oxidation by reduced natural organic matter in anoxic environments. Environ. Sci. Technol. 46, 292–299. https://doi.org/10.1021/es203402p.

Živković, I., Fajon, V., Kotnik, J., Shlyapnikov, Y., Obu Vazner, K., Begu, E., Šestanović, S., Šantić, D., Vrdoljak, A., Jozić, S., Šolić, M., Lušić, J., Veža, J., Kušpilić, G., Ordulj, M., Matić, F., Grbec, B., Bojanić, N., Ninčević Gladan, Ž., Horvat, M., 2019. Relations between mercury fractions and microbial community components in seawater under the presence and absence of probable phosphorus limitation conditions. J. Environ. Sci. 75, 145–162. https://doi.org/10.1016/j.jes.2018.03.012.